Synthesis and down-conversion luminescence of $Ba_4Y_3F_{17}$:Yb:Pr solid solutions for photonics

S. V. Kuznetsov[1], A. S. Nizamutdinov[2], M. N. Mayakova[1], V. V. Voronov[1], E. I. Madirov[2],
A. R. Khadiev[2], D. A. Spassky[3], I. A. Kamenskikh[4], A. D. Yapryntsev[5], V. K. Ivanov[5],
M. A. Marisov[2], V. V. Semashko[2], P. P. Fedorov[1]

[1]Prokhorov General Physics Institute of the Russian Academy of Sciences,
38 Vavilov str., Moscow, 119991 Russia

[2]Kazan Federal University, 18 Kremljovskaya, Kazan, 420008 Russia

[3]Skobeltsyn Institute of Nuclear Physics, Lomonosov Moscow State University,
Leninskie Gory, Moscow 119991, Russia

[4]Physics Faculty of Lomonosov Moscow State University, Leninskie Gory, Moscow 119991, Russia

[5]Kurnakov Institute of General and Inorganic Chemistry of the Russian Academy of Sciences,
31 Leninsky pr., Moscow,119991 Russia

kouznetzovsv@gmail.com

Single-phase powders of $Ba_4Y_3F_{17}$:Yb:Pr solid solutions with an average agglomerate size of 400 nm were synthesized by co-precipitation from aqueous solutions. It was shown that the down-conversion mechanism in the investigated samples was quantum cutting, with one photon absorbed by Pr^{3+} ions resulting in two photons emitted by Yb^{3+} ions. At first, overall the external quantum yield of down-conversion luminescence measured appeared to be relatively high, with a maximum value of 2.9 % for the $Ba_4Y_3F_{17}$:Pr(0.1 %):Yb(10 %) sample. It makes this compound promising for Si-based solar cells efficiency enhancement.

Keywords: synthesis, down-conversion, luminescence, solid solutions, photonics, fluorides.

1. Introduction

The forecast for the development of renewable energy [1], conducted by Fraunhofer ISE, showed that by 2030, humanity will reach the terawatt power generation capacity through photovoltaic devices. About 95 percent of this power will be generated by silicon solar panels. The cost of generating 1 kilowatt hour (kWh) of energy will be no higher than the cost of generating energy from fossils and nuclear power. One of the most significant drawbacks of Si-based solar cells is the low efficiency of power generation due to the limited range of high spectral susceptibility of crystalline silicon to sunlight. There are various options to increase the efficiency [2–8], including additional layers based on up-conversion (UC) [6, 7] and down-conversion [8] luminophores. These methods result in energy transfer from non-sensitive regions of the spectrum to crystalline silicon photosensitive range. The most efficient UC material excited at 980 nm is β-$NaYF_4$:21.4%Yb:2.2%Er with a reported photoluminescence quantum yield (PLQY) 10.5 % at pump power density P=35 W/cm^2 [9]. Other efficient UC materials described in the literature include BaY_2ZnO_5:7%Yb:3%Er with PLQY=5 % at P=2.2 W/cm^2 [10], La_2O_2S:9%Yb:1%Er with PLQY=5.8 % at P=13 W/cm^2 [11] and SrF_2:Yb(2 mol.%):Er(2 mol%) with PLQY=2.8 % at 10 W/cm^2 [7]. The phenomenon of quantum cutting is one of the down-conversion mechanisms, which allows one to transform the blue pump radiation to near infrared with an efficiency of more than 100 %. It was previously shown, that one of the most promising from the point of view of high quantum energy transfer efficiency is the ytterbium-praseodymium doping pair [12–17]. Previously, we studied solid solutions based on calcium fluoride and strontium fluoride doped with praseodymium and ytterbium [18, 19]. The best result was achieved for a solid solution based on SrF_2, which demonstrated an energy transfer coefficient of more than 100 % and a quantum yield of 1.1 % [18]. Usually, the luminescence efficiency increases with the transition to heavier matrices and with reduced symmetry. In this connection, it was logical to proceed to the study of fluorite solid solutions based on barium fluoride. It was previously shown that it was impossible to synthesize single-phase solid solutions $Ba_{1-x}R_xF_{2+x}$ (R – rare earth elements) by co-precipitation technique [20–22], since two-phase samples were synthesized. It is possible to synthesize $Ba_{1-x}R_xF_{2+x}$ solid solutions by high temperature melting technique, while fluorite-related trigonal

distorted $Ba_4Y_3F_{17}$ single-phases are synthesized from aqueous solutions [20–23]. The aim of this work was to study the synthesis and spectral-luminescent characteristics of $Ba_4Y_3F_{17}$ solid solutions.

2. Experimental

$Ba_4(Y,Yb,Pr)_3F_{17}$ samples were synthesized by co-precipitation from aqueous solutions as reported elsewhere [21, 24]. We used 99.99 wt% pure ytterbium, yttrium and praseodymium nitrate hexahydrates, barium nitrate (all reagents were manufactured by LANHIT, Russia), 99.99 wt% pure dihydrate potassium fluoride (REACHEM, Russia) and double distilled water as starting materials without further purification. Preliminary, the potassium fluoride was dried at 350°C for 3 hours. 0.08 M aqueous solutions of barium nitrate and rare earth nitrate were added dropwise to potassium fluoride (0.16 M) with intense stirring. Potassium fluoride was taken with a 50 % excess from stoichiometry. The process was carried out according to the following reaction:

$$4Ba(NO_3)_2 + 3R(NO_3)_3 + 17KF = Ba_4R_3F_{17} \downarrow +17KNO_3, \quad R = Y, Yb, Pr.$$

The resulting precipitates were dried at 45°C and annealed at 600°C. As a result, single-phase powders of $Ba_4(Y,Yb,Pr)_3F_{17}$ solid solutions were synthesized.

The samples were analyzed by X-ray powder diffraction on a Bruker D8 Advance (CuKα radiation) diffractometer. The unit cell parameters were calculated by TOPAS software (R_{wp} <10). Particle size, morphology and composition of the samples were analyzed by a Carl Zeiss NVision 40 scanning electron microscope equipped with an EDX detector.

Diffuse reflection spectra were recorded by a Thorlabs IS200 integrating sphere and a StellarNet EPP2000 spectrometer equipped with deuterium and halogen lamps. Luminescence and luminescence excitation spectra were measured using specialized setup for luminescence spectroscopy. A 150 W Xe lamp combined with monochromator MDR-206 was used as the excitation source. Luminescence was detected using an Oriel MS257 spectrograph equipped with Marconi 30–11 CCD detector. Also the luminescence was recorded by a StellarNet spectrometer with a spectral resolution of 0.5 nm and excited with 445 nm continuous wave laser diode. Luminescence kinetics were recorded with the use of MDR-23 equipped with FEU-100 and FEU-62 photomultipliers as detectors for UV-visible and IR spectral ranges, respectively. The time scanning for luminescence kinetics registration was carried out by two digital oscilloscopes: a BORDO oscilloscope with a bandwidth of 200 MHz, dynamic range of 10 bits, and a Tektronix DPO7354 oscilloscope with a bandwidth of 3.5 GHz, dynamic range of 8 bits. Pulsed excitation was arranged from OPO system Lotis TII LT2211 with 7 ns pulse duration and 10 Hz pulse repetition rate. The quantum yield of down-conversion luminescence was measured directly using a Thorlabs IS200 integrating sphere with previously-reported methods [25]. The radiation from the integrating sphere was transferred to a StellarNet spectrometer by optical fiber. The spectral characteristics of the recording system were calibrated with the use of TRSh-2850 and DRGS-12 lamps. All measurements were performed at 300 K.

3. Samples characterization

X-ray powder diffraction patterns of 45°C-dried $Ba_4(Y,Yb,Pr)_3F_{17}$ solid solutions are presented in Fig. 1a. The synthesis was carried out by the co-precipitation from aqueous solutions, and as a result, the particles have physically and chemically adsorbed water on their surfaces. It leads to the quenching of luminescence. The effect of annealing on the increase in luminescence intensity was previously demonstrated for both up-conversion and down-conversion phosphors in [19]. Thermal treatment was performed in the platinum crucible under air at 600°C for 1 hour. Annealing has resulted in a significant narrowing of the XRD peaks in comparison to the samples dried at 45°C (Fig. 1b).

Sobolev and Tkachenko [26] constructed phase diagrams of the BaF_2–RF_3 systems from melting points to 800°C for R=Sm–Lu and up to 900°C for R=La–Nd. In all systems, extensive regions of $Ba_{1-x}R_xF_{2+x}$ solid solutions with fluorite structure (space group Fm3m) are formed. The maximum is x=0.50±0.02 for R=La–Nd and decreases with decreasing ionic radius of R^{3+}. Fluorite-related phases of variable composition $Ba_{4\pm x}R_{3\pm x}F_{17\pm x}$ with a structure derived from fluorite (hexagonal crystal symmetry, space group R-3), formed in a concentration range of 40–45 mol.% RF$_3$, detected in systems with R=Sm–Lu. These phases melt incongruently for R=Tb–Lu, Y and decay in the solid state for R=Sm–Gd. A detailed consideration of the crystal structure of such phases for R=Y, Yb was carried out in [27], where a hexagonal structure with the ideal formula $Ba_4Y_3F_{17}$ was confirmed for them. It is shown that this hexagonal structure is a distortion of the cubic lattice of barium fluoride. However, the degree of this distortion is small, and on the X-ray powder patterns, the corresponding cleavage of the main reflexes is very weak. In accordance with this, the Table 1 presents only the data for the cubic sub-cell. The unit cell parameters (a) and coherent scattering range (D) have been calculated for $Ba_4(Y,Yb,Pr)_3F_{17}$ solid solutions (Table 1). The size of the coherent scattering region of samples dried at 45°C was about 20 nm. After annealing
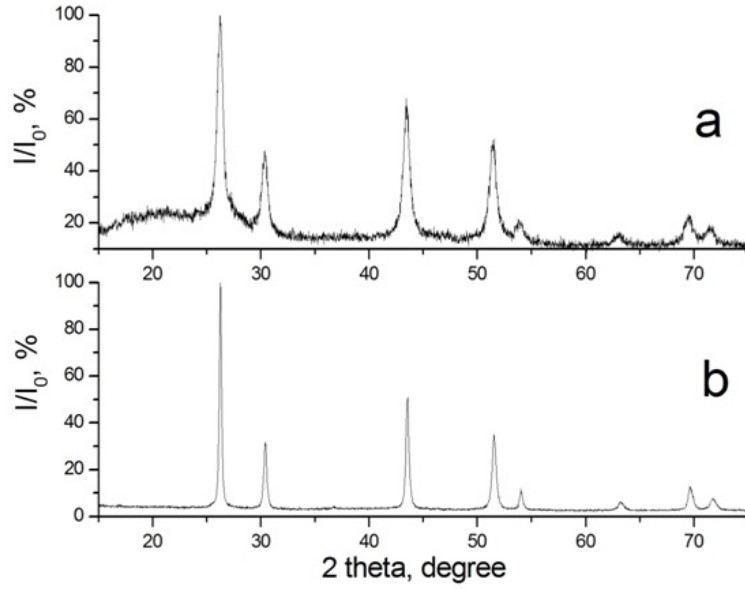
FIG. 1. X-ray powder diffraction patterns of $Ba_{0.5714}Y_{0.3282}Yb_{0.1}Pr_{0.0004}F_{2,4286}$ upon drying at $45°C$ (a) and annealing at $600°C$ (b)

at $600°C$, this value was increased several-fold. It should be noted that there is a regular decrease in the unit cell parameters with increasing ytterbium content in the crystal lattice. It is due to the fact that the ionic radius of ytterbium is smaller than that of yttrium according to the Shannon system [28].

TABLE 1. Unit cell parameters of $Ba_4(Y,Yb,Pr)_3F_{17}$ solid solutions

Compositions of the initial aqueous solution	After drying at $45°C$		After annealing at $600°C$	
	a, Å	D, nm	a, Å	D, nm
$Ba_{0.5714}Y_{0.3982}Yb_{0.03}Pr_{0.0004}F_{2,4286}$	5.9175(5)	20±1	5.8978(4)	>100
$Ba_{0.5714}Y_{0.3282}Yb_{0.1}Pr_{0.0004}F_{2,4286}$	5.9021(7)	14±1	5.8851(2)	70±6
$Ba_{0.5714}Y_{0.2782}Yb_{0.15}Pr_{0.0004}F_{2,4286}$	5.8818(6)	25±1	5.8710(3)	90±8
$Ba_{0.5714}Y_{0.3976}Yb_{0.03}Pr_{0.001}F_{2,4286}$	5.9118(6)	19±1	5.8905(2)	71±6
$Ba_{0.5714}Y_{0.3276}Yb_{0.1}Pr_{0.001}F_{2,4286}$	5.8997(6)	23±1	5.8800(3)	>100
$Ba_{0.5714}Y_{0.2776}Yb_{0.15}Pr_{0.001}F_{2,4286}$	5.8843(8)	21±1	5.8684(6)	>100

The particles of $Ba_4(Y,Yb,Pr)_3F_{17}$ solid solutions are agglomerates with an average particle size of 400 nm (Fig. 2). The change in size depending on the content of ytterbium and praseodymium is not substantial.

The composition of the samples has been determined by energy-dispersive analysis (Table 2). Yb content is higher than in the initial aqueous solutions. The yttrium content is the same as in the initial aqueous solutions. The barium content decreases with increasing ytterbium content, which is confirmed by the corresponding distribution coefficient. The appearance of potassium in the crystal lattice of this solid solution arises from the fluorinating agent. The absence of potassium in a number of samples indicates that its amount is less than the detection limit.

4. Spectral-kinetic characteristics

The diffusion reflection spectrum of $Ba_4Y_3F_{17}$:Pr(0.1 %):Yb(1.00 %) sample is shown in Fig. 3. The characteristic Pr^{3+} ions transitions from $^3H_4$ manifold to ^3P_J and $^1D_2$ states appear in the blue and red spectral regions correspondingly. However, the reflection spectrum is dominated by the transition from $^2F_{7/2}$ to $^2F_{5/2}$ states of Yb^{3+} ions at ~980 nm.
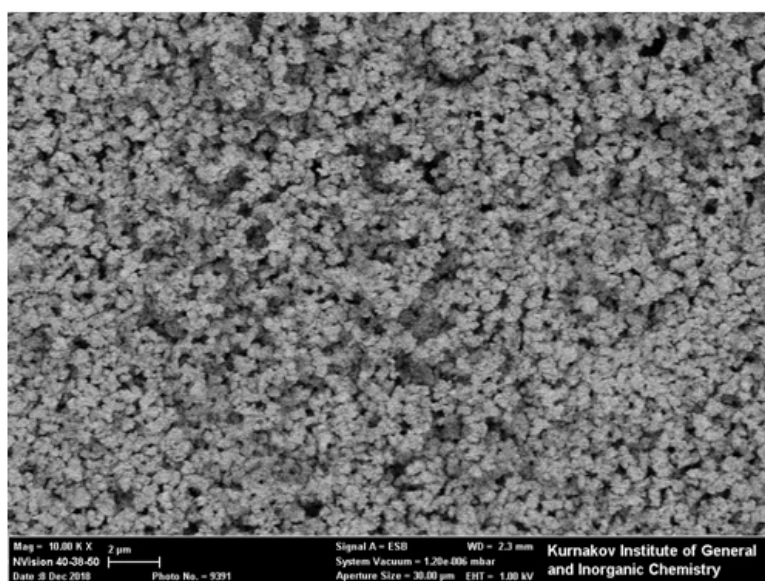
FIG. 2. SEM image of $Ba_4(Y,Yb,Pr)_3F_{17}$ powder annealed at $600°C$

TABLE 2. The energy-dispersive analysis of $Ba_4(Y,Yb,Pr)_3F_{17}$ solid solutions

Compositions of the initial aqueous solution	Composition of the solid solutions as determined by EDX*	Barium, yttrium and ytterbium distribution coefficients (EDX composition / Initial composition)
$Ba_{0.5714}Y_{0.3982}Yb_{0.03}Pr_{0.0004}F_{2,4286}$	$Ba_{0.5624}Y_{0.4026}Yb_{0.0350}F_{2,4376}$	0.98/1.01/1.16
$Ba_{0.5714}Y_{0.3282}Yb_{0.1}Pr_{0.0004}F_{2,4286}$	$Ba_{0.5380}Y_{0.3440}Yb_{0.1180}F_{2,4620}$	0.94/1.05/1.18
$Ba_{0.5714}Y_{0.2782}Yb_{0.15}Pr_{0.0004}F_{2,4286}$	$Ba_{0.5100}K_{0.0131}Y_{0.2814}Yb_{0.1961}F_{2,4644}$	0.89/1.01/1.30
$Ba_{0.5714}Y_{0.3976}Yb_{0.03}Pr_{0.001}F_{2,4286}$	$Ba_{0.5490}Y_{0.4140}Yb_{0.0370}F_{2,4510}$	0.96/1.04/1.23
$Ba_{0.5714}Y_{0.3276}Yb_{0.1}Pr_{0.001}F_{2,4286}$	$Ba_{0.5340}K_{0.0110}Y_{0.3300}Yb_{0.1250}F_{2,4440}$	0.93/1.00/1.25
$Ba_{0.5714}Y_{0.2776}Yb_{0.15}Pr_{0.001}F_{2,4286}$	$Ba_{0.5140}K_{0.0140}Y_{0.2830}Yb_{0.1890}F_{2,45800}$	0.90/1.02/1.26

*The praseodymium content is below the EDX detection limit

The luminescence spectra of the samples were investigated under excitation by 445 nm light, which corresponds to the excitation of Pr^{3+} ions and lies within efficient solar spectrum. All samples have exhibited luminescence of both Pr^{3+} and Yb^{3+} ions. In Fig. 4, the luminescence spectra are shown for $Ba_4Y_3F_{17}$:Pr(0.1 %) samples co-doped with 10 % and 15 % Yb.

The ions pair Pr^{3+} and Yb^{3+} often exhibit a quantum cutting effect, which consists in emission of two photons of Yb^{3+} luminescence as a result of absorption of one photon to ^3P_J manifold of Pr^{3+} ions. It is clearly seen from the comparison in the spectral range 400–650 nm of excitation spectrum monitored at 980 nm and diffusion reflection spectrum of the sample (see Fig. 5).

Excitation to ^3P_J manifold of Pr^{3+} ions may lead to two excited Yb^{3+} ions whereas energy of excitation to $^1D_2$ manifold of Pr^{3+} is not enough to achieve quantum cutting effect. From Fig. 5, we see qualitatively that the ratio of areas under lines $^3P_J/^1D_2$ is higher for excitation spectrum than that for reflectance of those which is the evidence of quantum cutting effect [29].

It is worth noting that the excitation spectrum was not corrected for the spectral sensitivity function because of the absence of a reference sample with constant quantum yield in the region 500–600 nm. However, the intensity
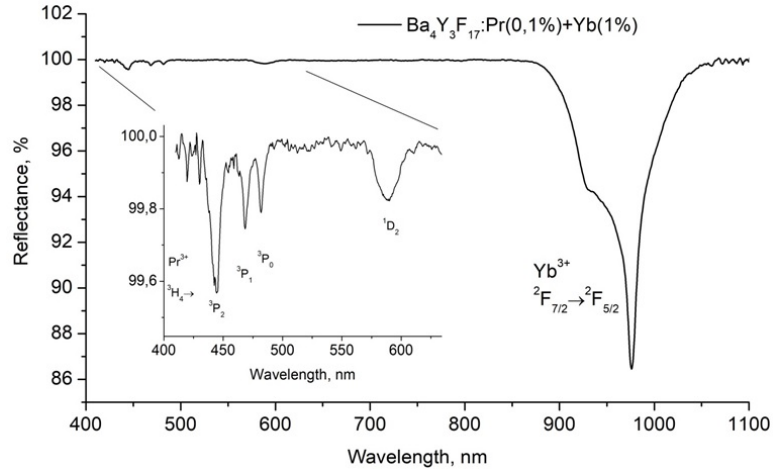
FIG. 3. Diffusion reflection spectrum of $Ba_4Y_3F_{17}$:Pr(0.1 %):Yb(1.0 %) powder sample. The inset shows the magnified visible spectral range reflection
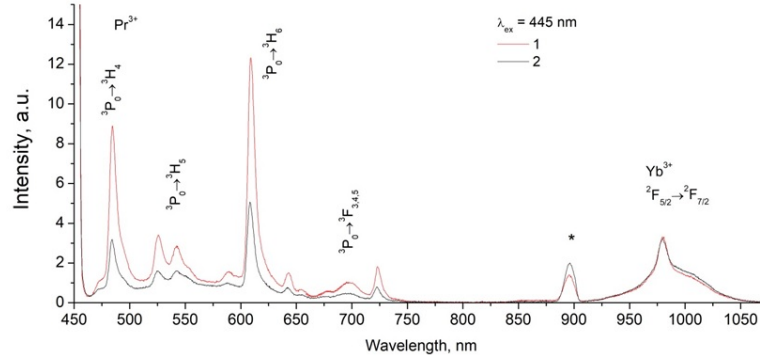
FIG. 4. Luminescence spectra of $Ba_4Y_3F_{17}$:Pr(0.1 %):Yb(10.00 %) (1) and $Ba_4Y_3F_{17}$:Pr(0.1 %):Yb(15.00 %) (2) powder samples excited by 445 nm CW laser light. The sign (*) indicates the second order observation of excitation light

of the excitation source at 590 nm is several times higher than that at 450 nm. Therefore, we expect even higher relative intensity for the group of lines in the region 440–500 nm after the correction. The presented spectra allow one to make a qualitative conclusion concerning the quantum cutting effect in the studied samples without any quantitative estimations on the efficiency of the process.

As a result, we clearly see the down-conversion luminescence of Yb^{3+} ions when samples are excited to $^3H_4$-$^3P_2$ transition of Pr^{3+} ions. The energy transfer features will inevitably appear in luminescence kinetics curves. The Pr^{3+} luminescence decays at 605 nm are shown in Fig. 6.

Curves in Fig. 6 indicate that the luminescence decay from ^3P_J manifold of Pr^{3+} ions is non-exponential, especially for the early stage of decay. We see that an increase in the Yb^{3+} ion concentration leads to quenching of Pr^{3+} luminescence, which speaks for non-radiative energy transfer. Due to the non-exponential character of decay, the average luminescence lifetimes were calculated with the use of formula (1):

$$t_{avg} = \frac{\int t^* I(t) dt}{\int I(t) dt}, \tag{1}$$

where $I(t)$ is the intensity of the decay curve, and t is time.

The results of calculation are presented in Table 3.

The luminescence lifetime values presented in Table 3 indicate the energy transfer from Pr^{3+} ions to Yb^{3+} ions. But also we see that there is some increase for Pr^{3+} luminescence lifetime with the increase of Pr^{3+} content. As this is seen in double doped samples this can be the evidence of certain cross-relaxation process resulting in energy back transfer from Yb^{3+} to Pr^{3+} as transitions $^2F_{7/2}$ to $^2F_{5/2}$ of Yb^{3+} ions and $^1G_4$-$^3P_0$ of Pr^{3+} ions are almost equal in energy. These peculiarities are also shown in Yb^{3+} luminescence kinetics.
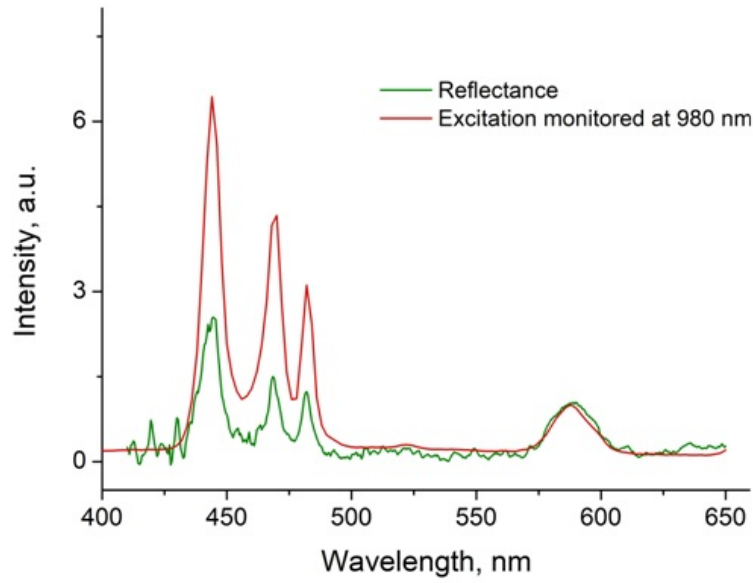
FIG. 5. Excitation spectrum monitored and 980 nm and diffusion reflection spectrum for Ba$_4$Y$_3$F$_{17}$:Pr(0.1 %):Yb(10.0 %) powder sample both normalized to the maximum of ^{3}H$_4$-^{1}D$_2$ transition. Higher values of intensity of excitation lines correspondent to ^{3}H$_4$-^{3}P$_J$ transitions compared to normalized values of reflectance of those illustrate the quantum cutting effect
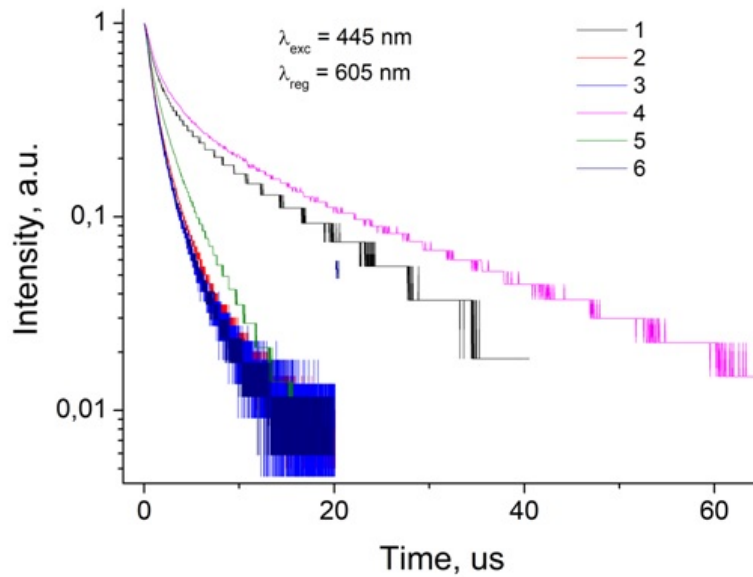

FIG. 6. Luminescence decay curves of Ba$_4$Y$_3$F$_{17}$:Pr(X %):Yb(Y %) samples excited at 445 nm registered at 605 nm. Here X/Y corresponds to 0.04/3.00 (1), 0.04/10.00 (2), 0.04/15.00 (3), 0.1/3.00 (4), 0.1/10.00 (5), 0.1/15.00 (6)

TABLE 3. Average luminescence lifetime of Pr^{3+} detected at 605 nm in Ba$_4$Y$_3$F$_{17}$:Pr:Yb powder under 445 nm excitation, μs

Yb and Pr content, mol.%	Yb (3.0 %)	Yb (10.0 %)	Yb (15.0 %)
Pr (0.04 %)	9.0	2.8	2.5
Pr (0.1 %)	15.9	3.0	2.3
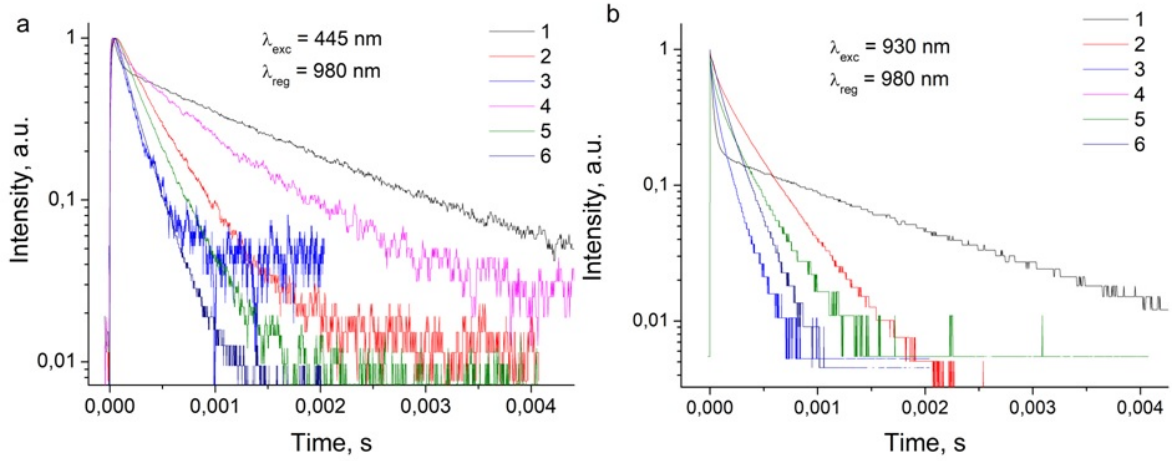
FIG. 7. Luminescence decay curves of $Ba_4Y_3F_{17}$:Pr(X %):Yb(Y %) samples registered at 980 nm excited at 445 nm (a) and 930 nm (b). Here X/Y corresponds to 0.04/3.00 (1), 0.04/10.00 (2), 0.04/15.00 (3), 0.1/3.00 (4), 0.1/10.00 (5), 0.1/15.00 (6)

The luminescence decays of Yb^{3+} ions both under 445 nm excitation (Fig. 7a) and 980 nm excitation (Fig. 7b) appear to be non-exponential due to non-radiative quenching and also due to sensitized character of excitation for the latter. The luminescence lifetime was estimated as the average lifetime by formula (1) also, the results are presented in Table 4.

TABLE 4. Average luminescence lifetime of Yb^{3+} detected at 980 nm in $Ba_4Y_3F_{17}$:Pr:Yb powder under 445 and 930 nm excitation

Avg. time, ms	Yb 3.0 %		Yb 10.0 %		Yb 15.0 %	
Excitation, nm	**445**	**930**	**445**	**930**	**445**	**930**
Pr 0.04 %	1.47	1.48	0.345	0.320	0.159	0.124
Pr 0.10 %	0.729	0.756	0.266	0.248	0.184	0.167

Results of calculation in Table 4 show that Yb^{3+} ions exhibit strong concentration quenching. Also, it is important to note that the increase of Pr^{3+} ions also leads to a decrease in Yb^{3+} luminescence lifetime, which is seen for high concentrations of Yb^{3+} ions. It is a known feature of Pr/Yb ions pair when Yb^{3+} ions transfer their excitation to $^1G_4$ manifold of Pr^{3+} ions [19, 29]. At the same time, the down-conversion mechanism results in a bit longer luminescence lifetime when excited at 445 nm. From Fig. 7a, we can see that the luminescence of Yb^{3+} under 445 nm pulse excitation exhibits some build-up which was not observed in kinetics with direct Yb^{3+} excitation (Fig. 7b). This build-up time is on the same order of magnitude with the $^3P_0$ manifold of Pr^{3+} lifetime, which speaks for a rate of energy transfer to Yb^{3+} as high as on the order of 10^6 s^{-1}.

The luminescence spectrum corrected for the spectral sensitivity of our detection system allows estimation of energy transfer efficiency [19]. Ratios of integral luminescence intensity of Yb^{3+} ions to the integral luminescence intensity of the whole emission spectrum of the sample can be the measure of energy transfer coefficient between sensitizer (Pr^{3+}) and activator (Yb^{3+}) ions together with their concentration quenching processes (2):

$$q^E = \frac{\int I^{Yb}(\lambda)d\lambda}{\int (I^{Yb}(\lambda) + I^{Pr}(\lambda))d\lambda}, \tag{2}$$

where $I^{Yb}(\lambda)$ is the Yb^{3+} ion luminescence intensity, $I^{Pr}(\lambda)$ is the Pr^{3+} ion luminescence intensity. The corresponding calculation results are presented in Table 5.

From Table 5, we see that the energy transfer efficiency from Pr^{3+} ions to Yb^{3+} ions reaches 74 % for $Ba_4Y_3F_{17}$:Pr(0.1 %):Yb(15.0 %) powder sample which is relatively large and speaks for high efficiency of the down-conversion system, since Yb^{3+} luminescence is not quenched at a high rate at this concentration.

TABLE 5. Energy transfer from Pr^{3+} to Yb^{3+} ions in Ba$_4$Y$_3$F$_{17}$ powder estimated from luminescence spectra, %

Yb and Pr content, mol.%	Yb (10.0 %)	Yb (15.0 %)
Pr (0.04 %)	54	58
Pr (0.10 %)	58	74

The external efficiency of down conversion was investigated for studied samples by means of measurement of quantum yield of Yb^{3+} ions luminescence excited at 445 nm in the integrating sphere attached to the spectrometer by the technique described in [25]. Results are presented in the Table 6.

TABLE 6. Estimated external quantum yield of down-conversion luminescence of Yb^{3+} ions of Ba$_4$Y$_3$F$_{17}$:Pr:Yb powder samples measured in integrating sphere, %

Yb and Pr content, mol.%	Yb (10.0 %)	Yb (15.0 %)
Pr (0.04 %)	0.8	0.8
Pr (0.1 %)	2.9	2.6

The results of external quantum yield measurement of down conversion luminescence in Ba$_4$Y$_3$F$_{17}$:Pr:Yb powder samples speak for the potential of the compound. Values of quantum yield above 2 % are relatively high compared to CaF$_2$:Pr:Yb and SrF$_2$:Pr:Yb solid solutions with its values lower than 1 [18, 19], or upconverter materials for solar cells (about 1 %) [30].

5. Conclusions

Single-phase powders of Ba$_4$Y$_3$F$_{17}$:Yb:Pr solid solutions with an average agglomerate size of 400 nm were synthesized by co-precipitation from aqueous solutions. The down-conversion luminescence was investigated in Ba$_4$Y$_3$F$_{17}$ co-doped with Pr^{3+} and Yb^{3+} ions. When excited to ^{3}P$_J$ manifold of Pr^{3+} ions, the samples exhibited luminescence of both Pr^{3+} and Yb^{3+} ions. The energy transfer efficiency appeared to be 74 % for Pr^{3+} 0.1 % and Yb^{3+} 15.0 %, which appears to be efficient, since Yb^{3+} luminescence is still not strongly quenched at this concentration. It was shown that the down-conversion mechanism in the investigated samples is quantum cutting, when one photon absorbed by Pr^{3+} ions results in two photons emitted by Yb^{3+} ions. At the same time, the energy back transfer from Yb^{3+} to Pr^{3+} was observed apparently through resonant energy transfer involving ^{2}F$_{7/2}$–^{2}F$_{5/2}$ of Yb^{3+} ions and ^{1}G$_4$-^{3}P$_0$ of Pr^{3+} ions transitions. Overall, the external quantum yield of down-conversion luminescence measured in our study appeared to be relatively high, with a maximum value of 2.9 % for Ba$_4$Y$_3$F$_{17}$:Pr(0.1 %):Yb(10.0 %) sample, which makes this compound promising for Si-based solar cell efficiency enhancement.

Acknowledgements

References

[1] Weber E.R. Photovoltaics moving into the terawatt age. *Proc. SPIE* 10368, Next Generation Technologies for Solar Energy Conversion VIII, 1036803, 25 August 2017, DOI: 10.1117/12.2277978.

[2] Green M.A., Bremner S.P. Energy conversion approaches and materials for high-efficiency photovoltaics. *Nature Mater.*, 2017, **16**, P. 23–34.

[3] Han G., Zhang S., Boix P.P., Wong L.H., Sun L., Lien S.Y. Towards high efficiency thin film solar cells. *Progress in Materials Science*, 2017, **87**, P. 246–291.

[4] Engelhart P., Wendt J., Schulze A., Klenke C., Mohr A., Petter K., Stenzel F., Hörnlein S., Kauert M., Junghänel M., Barkenfelt B., Schmidt S., Rychtarik D., Fischer M., Müller J.W., Wawer P. R&D pilot line production of multi-crystalline Si solar cells exceeding cell efficiencies of 18 %. *Energy Procedia*, 2011, **8**, P. 313–317.

[5] Yang J., Myong S.Y., Lim K.S. Novel ultrathin LiF interlayers for efficient light harvesting in thin-film Si tandem solar cells. *Solar Energy*, 2015, **114**, P. 259–267.

[6] Fischer S., Ivaturi A., Jakob P., Krämer K.W., Martin-Rodriguez R., Meijerink A., Richards B., Goldschmidt J.Ch. Upconversion solar cell measurements under real sunlight. *Optical Materials*, 2018, **84**, P. 389–395.

[7] Kuznetsov S., Ermakova Yu., Voronov V., Fedorov P., Busko D., Howard I.A., Richards B.S., Turshatov A. Up-conversion Quantum Yield of $SrF_2:Yb^{3+}$, Er^{3+} Sub-micron Particles Prepared by Precipitation from Aqueous Solution. *J. Mater. Chem. C.*, 2018, **6**, P. 598–604.

[8] Huang X., Han S., Huang W., Liu X. Enhancing solar cell efficiency: the search for luminescent materials as spectral converters. *Chem. Soc. Rev.*, 2013, **42**, P. 173–201.

[9] Kaiser M., Wurth C., Kraft M., Hyppanen I., Soukka T., Resch-Genger U. Power-dependent upconversion quantum yield of $NaYF_4:Yb^{3+},Er^{3+}$ nano- and micrometer-sized particles - measurements and simulations. *Nanoscale*, 2017, **9**, P. 10051–10058.

[10] Etchart I., Huignard A., Berard M., Nordin M.N., Hernandez I., Curry R.J., Gillin W.P., Cheetham A.K. Oxide phosphors for efficient light upconversion: Yb^{3+} and Er^{3+} co-doped Ln_2BaZnO_5 (Ln = Y, Gd). *J. Mater. Chem.*, 2010, **20**, P. 3989–3994.

[11] Pokhrel M., Kumar G.A., Sardar D.K. Highly efficient NIR to NIR and VIS upconversion in Er^{3+} and Yb^{3+} doped in M_2O_2S (M = Gd, La, Y). *J. Mater. Chem. A*, 2013, **1**, P. 11595–11606.

[12] Piper W.W., DeLuca J.A., Ham F.S. Cascade fluorescent decay in P^{3+}-doped fluorides: Achievement of a quantum yield greater than unity for emission of visible light. *J. Lumin.*, 1974, **8**, P. 344–348.

[13] Lee T.-J., Luo L.-Y., Cheng B.-M., Diau W.-G., Chen T.-M. Investigation of Pr^{3+} as a sensitizer in quantum-cutting fluoride phosphors. *Appl. Phys. Lett.*, 2008, **92**, P. 081106-1–081106-3.

[14] Van der Ende B.M., Aarts L., Meijerink A. Near-infrared quantum cutting for photovoltaics. *Adv. Mater.*, 2009, **21**, P. 3073–3077.

[15] Song P., Jiang C. Modeling of down converter based on Pr^{3+}–Yb^{3+} codoped fluoride glasses to improve sc-Si solar cells efficiency. *AIP Adv.*, 2012, **2**, P. 042130-1–042130-10.

[16] Zhang L., Xu J., Hu Y., Chen G., Wang Zh. Near-infrared quantum cutting in Pr^{3+}–Yb^{3+} co-doped oxyfluoride glass ceramics containing CaF_2 nanocrystals. *J. Wuhan University of Technology-Mater. Sci. Ed.*, 2013, P. 455–459.

[17] Shao W., Chen G., Ohulchanskyy T.Y., Yang Ch., Agren H., Prasad P.N. A core – multiple shell nanostructure enabling concurrent upconversion and quantum cutting for photon management. *Nanoscale*, 2017, **9**, P. 1934–1941.

[18] Kuznetsov S.V., Proydakova V.Yu., Morozov O.A., Gorieva V.G., Marisov M.A., Voronov V.V., Yapryntsev A.D., Ivanov V.K., Nizamutdinov A.S., Semashko V.V., Fedorov P.P. Synthesis and quantum yield investigations of the $Sr_{1-x-y}Pr_xYb_yF_{2+x+y}$ luminophores for photonics. *Nanosystems: physics, chemistry, mathematics*, 2018, **9**(5), P. 663–668.

[19] Kuznetsov S.V., Morozov O.A., Gorieva V.G., Mayakova M.N., Marisov M.A., Voronov V.V., Yapryntsev A.D., Ivanov V.K., Nizamutdinov A.S., Semashko V.V., Fedorov P.P. Synthesis and luminescence studies of $CaF_2:Yb:Pr$ solid solutions powders for photonics. *J. Fluor. Chem.*, 2018, **211**, P. 70–75.

[20] Kuznetsov S.V., Fedorov P.P., Voronov V.V., Samarina K.S., Ermakov R.P., Osiko V.V. Synthesis of $Ba_4R_3F_{17}$ (R stands for Rare-Earth Elements) Powders and Transparent Compacts on Their Base. *Russ. J. Inorg. Chem.*, 2010, **55**(4), P. 484–493.

[21] Fedorov P.P., Mayakova M.N., Kuznetsov S.V., Voronov V.V., Ermakov R.P., Samarina K.S., Popov A.I., Osiko V.V. Co-precipitation of yttrium and barium fluorides from aqueous solutions. *Mater. Res. Bull.*, 2012, **47**, P. 1794–1799.

[22] M. Karbowiak, J. Cichos Does $BaYF_5$ nanocrystals exist? - The BaF_2-YF_3 solid solution revisited using photoluminescence spectroscopy. *Journal of Alloys and Compounds*, 2016, **673**, P. 258–264.

[23] Li T., Li Y., Luo R., Ning Zh., Zhao Y., Liu M., Lai X., Zhong Ch., Wang Ch., Zhang J., Bi J., Gao D. Novel $Ba(Gd_{1-x}Y_x)_{0.78}F_5$: 20 mol% Yb^{3+}, 2 mol% Tm^{3+} (0≤x≤1.0) solid solution nanocrystals: A facile hydrothermal controlled synthesis, enhanced upconversion luminescent and paramagnetic properties. *J. Alloys Comp.*, 2018, **740**, P. 1204–1214.

[24] Fedorov P.P., Kuznetsov S.V., Mayakova M.N., Voronov V.V., Ermakov R.P., Baranchikov A.E., Osiko V.V. Coprecipitation from aqueous solutions to prepare binary fluorides. *Russ. J. Inorg. Chem.*, 2011, **56**(10), P. 1525–1531.

[25] Yasyrkina D.S., Kuznetsov S.V., Ryabova A.V., Pominova D.V., Voronov V.V., Ermakov R.P., Fedorov P.P. Dependence of quantum yield of up-conversion luminescence on the composition of fluorite-type solid solution $NaY_{1-x-y}Yb_xEr_yF_4$. *Nanosystems: physics, chemistry, mathematics*, 2013, **4**(5), P. 648–656.

[26] Sobolev B.P., Tkachenko N.L. Phase diagrams of $BaF_{2-}(Y, Ln)F_3$ systems. *J. Less. Common Met.*, 1982, **85**, P. 155–170.

[27] Maksimov B.A., Solans Kh., Dudka A.P., et al. The fluorite-matrix-based $Ba_4R_3F_{17}$ (R=Y,Yb) crystal structure. Ordering of cations and specific features of the anionic motif. *Crystallogr. Rep.*, 1996, **41**(1), P. 50.

[28] Shannon R.D. Revised Effective Ionic Radii and Systematic Studies of Interatomic Distances in Halides and Chalcogenides. *Acta Cryst.*, 1976, **A32**, P. 751–767.

[29] Aarts L., van der Ende B., Reid M., Meijerink A. Downconversion for Solar Cells in $YF_3:Pr^{3+}$, Yb^{3+}. *Spectroscopy Letters*, 2010, **43**, P. 373–381.

[30] de Wild J., Meijerink A., Rath J.K., van Sark W.G.J.H.M., Schropp R.E.I. Upconverter solar cells: materials and applications. *Energy Environ. Sci.*, 2011, **4**, P. 4835–4848.